

Study of *Dst*/ring current recovery times using the WINDMI model

S. Patra,¹ E. Spencer,¹ W. Horton,² and J. Sojka³

Received 29 June 2010; revised 15 November 2010; accepted 29 November 2010; published 17 February 2011.

[1] We use the WINDMI model of the nightside magnetosphere to investigate the contributions of ring current, magnetotail current, and magnetopause current on the observed two-phase decay of the *Dst* index. For the analysis, several geomagnetic events in the period 2000–2007 were identified, during which the interplanetary magnetic field (IMF B_z) turns northward during the early recovery phase of the storm. The *Dst* recovery rate for these events were first estimated for either of two possible periods: by assuming an initial fast decay phase or by assuming an overall decay for the entire duration of storm. The recovery rates were estimated by matching *Dst* and *Dst** data against WINDMI model predictions. We consistently found an increase in the *Dst* recovery times when a shorter initial decay phase was chosen as compared to an overall decay phase, thus, confirming the observations of two-phase decay and indicating the possibility of contributions from faster initial decay mechanisms. We then modified the *Dst* index as estimated by the WINDMI model to include contributions from the cross-tail current and magnetopause currents. The modified *Dst* was then optimized for all the events. The optimized results correlate very well to the *Dst* dynamics and indicate that under northward IMF B_z conditions and during the early recovery phase of a storm; contributions from the geotail currents to the fast initial decay of the *Dst* index are important, while the slower recovery of *Dst* in the later phases of the storm are due to the charge exchange dominated ring current decay.

Citation: Patra, S., E. Spencer, W. Horton, and J. Sojka (2011), Study of *Dst*/ring current recovery times using the WINDMI model, *J. Geophys. Res.*, 116, A02212, doi:10.1029/2010JA015824.

1. Introduction

[2] The disturbance storm time (*Dst*) index has been widely used as an indicator of geomagnetic activity. *Dst**, which is obtained after removing the contributions from magnetopause currents, induced currents in the conducting Earth, and the quiet time ring current, is assumed to represent the ring current (RC) activity during geomagnetic storms. The ring current particles are energized during a geomagnetic storm which corresponds to a decrease in the *Dst* index. The decay time of the ring current energy is important because the particle injection rate cannot be determined without sufficient knowledge of the decay parameter. It has been observed that the *Dst* decay following a geomagnetic storm shows a two-phase pattern, a period of fast decay followed by a phase where the *Dst* returns to its quiet time value gradually [Takahashi *et al.*, 1990; Feldstein and Dremukhina, 2000; Kozyra *et al.*, 1998].

[3] There are many theories that have been proposed to explain the observations. It has been proposed that differ-

ential decay rates of different ion species may lead to the two-phase decay as explained in the review paper by *Daglis et al.* [1999]. This claim was questioned by *Liemohn and Kozyra* [2005], whose idealized simulations of ring current decay show that for realistic plasma boundary conditions, a two-phase decay can only be created by the transition from flow-out losses when open drift lines are converted to closed ones in a weakening convection electric field resulting in the charge exchange dominance of ring current loss. In a study by *Jordanova et al.* [2003] it was shown that the fast initial ring current decay is controlled not only by the decreased convection electric field, the dayside outflow through the magnetopause, and the internal loss processes, but also by the time-varying nightside inflow of plasma from the magnetotail.

[4] An alternative explanation is that during the recovery phase of the magnetic storm, the *Dst* decay is controlled by the decay of two different currents: the ring current and the magnetospheric tail current [Alexeev *et al.*, 1996; Feldstein and Dremukhina, 2000]. Recent work of *Kalegaev and Makarenkov* [2008] indicates that the ring current becomes the dominant *Dst* source during severe magnetic storms, but during moderate storms its contribution to *Dst* is comparable with the tail current's contribution.

[5] According to *Kozyra et al.* [2002] and *Takahashi et al.* [1990], an abrupt northward turning of the interplanetary magnetic field traps ring current ions on closed trajectories,

¹Center for Space Engineering, Utah State University, Logan, Utah, USA.

²Space and Geophysics Laboratory, University of Texas at Austin, Austin, Texas, USA.

³CASS, Utah State University, Logan, Utah, USA.

turning off sources and fast flow-out losses, resulting in charge exchange losses being the dominant loss process. Under these conditions, it is expected that there is no distinctive two-phase decay but a single phase with a slowly increasing decay time period as species with short charge exchange collision lifetimes are preferentially removed.

[6] *Mitchell et al.* [2001] have used energetic neutral atom (ENA) images of the Earth's inner magnetosphere to compare the ring current morphology during the Bastille day event and a moderate event on 10 June 2000 for which the IMF B_z gradually turned northward. They confirmed that the contribution to the ring current in the small, 10 June storm and associated substorms was much further away from Earth, and much more dependent on open drift path dynamics, than in the larger Bastille storm where the ions contributing to *Dst* drifted primarily on closed paths.

[7] Based on ion flux measurements by the Geotail satellite *Keika et al.* [2005] have suggested, that near the earthward side of the low latitude boundary layer, the drift governing the ion outflow is mainly the ∇B drift. They concluded that the ion outflow contributes significantly to the rapid decay of the ring current, even in the case of a sudden northward turning of the interplanetary magnetic field. However, *Lee et al.* [2005] have reported that the magnetospheric compression by a dynamic pressure (P_{dyn}) enhancement usually causes particle fluxes to increase globally around the Earth. They argued that changes in the particle flux at a given energy channel due to the compressional effect of a P_{dyn} enhancement must, in general, be determined by a combination of adiabatic acceleration and the spatial (radial) profile of the source particle distribution at constant first and second adiabatic invariants.

[8] In this work we identify geomagnetic storms in the period 2000–2007 where the IMF B_z abruptly turns northward during the early recovery phase of the storm. For these events ring current particles should be trapped and the initial fast decay of *Dst* due to flow out losses should not be dominant. We use the WINDMI model to estimate the decay period of *Dst* and *Dst** indices for different periods of the decay phase.

[9] The WINDMI model, which is described in section 2, assigns a fixed decay rate for the ring current particles. We use the fixed decay rate to compare the decay times obtained by either assuming an early recovery phase or by assuming a decay over the entire duration of the storm for analysis, to infer if different decay rates are observed.

[10] A Genetic Algorithm (GA) optimization procedure is used for all the curve fitting done in this work. The algorithm is explained in section 3. The test for differential decay rates of the *Dst* and the events used in this study are explained in section 4.1. We assume that the ion outflow during periods of northward magnetic field is not as significant as during southward IMF conditions.

[11] The contribution from other magnetospheric current systems to *Dst* is investigated in section 5 to estimate their effect on the recovery times of the index. Magnetic perturbations at the surface of the Earth due to the cross-tail current is taken to be proportional to the geotail current value evaluated by the WINDMI model. The contribution of magnetopause currents to the *Dst* index is assumed to be a function of the solar wind dynamic pressure. The expressions used for the magnetopause contributions are explained

in section 5. A parameterized model for the *Dst* index is obtained by including contributions from magnetopause currents, ring current and the tail current. The modeled magnetic disturbances are optimized for all the storms using a genetic algorithm to obtain solutions that simultaneously have least mean square fit to the AL and *Dst* indices weighted appropriately.

2. The WINDMI Model

[12] The plasma physics based WINDMI model uses the solar wind dynamo voltage, V_{sw} , generated by a particular solar wind-magnetosphere coupling function to drive eight ordinary differential equations describing the transfer of power through the geomagnetic tail, the ionosphere and the ring current. The WINDMI model is described in some detail by *Doxas et al.* [2004], *Horton et al.* [2005], and more recently, by *Spencer et al.* [2007]. The equations of the model are given by

$$L \frac{dI}{dt} = V_{sw}(t) - V + M \frac{dI_1}{dt} \quad (1)$$

$$C \frac{dV}{dt} = I - I_1 - I_{ps} - \Sigma V \quad (2)$$

$$\frac{3}{2} \frac{dp}{dt} = \frac{\Sigma V^2}{\Omega_{cps}} - u_0 p K_{\parallel}^{1/2} \Theta(u) - \frac{p V A_{eff}}{\Omega_{cps} B_{tr} L_y} - \frac{3p}{2\tau_E} \quad (3)$$

$$\frac{dK_{\parallel}}{dt} = I_{ps} V - \frac{K_{\parallel}}{\tau_{\parallel}} \quad (4)$$

$$L_I \frac{dI_1}{dt} = V - V_I + M \frac{dI}{dt} \quad (5)$$

$$C_I \frac{dV_I}{dt} = I_1 - I_2 - \Sigma_I V_I \quad (6)$$

$$L_2 \frac{dI_2}{dt} = V_I - (R_{pre} + R_{A2}) I_2 \quad (7)$$

$$\frac{dW_{rc}}{dt} = R_{pre} I_2^2 + \frac{p V A_{eff}}{B_{tr} L_y} - \frac{W_{rc}}{\tau_{rc}} \quad (8)$$

The nonlinear equations of the model trace the flow of electromagnetic and mechanical energy through eight pairs of transfer terms. The remaining terms describe the loss of energy from the magnetosphere-ionosphere system through plasma injection, ionospheric losses and ring current energy losses.

[13] In the differential equations the coefficients are physical parameters of the magnetosphere-ionosphere system. The quantities L , C , Σ , L_I , C_I and Σ_I are the magnetospheric and ionospheric inductances, capacitances, and conductances, respectively. A_{eff} is an effective aperture for particle injection into the ring current, that on the duskside merges with what is known as the Alfvén layer [*Doxas et al.*, 2004]. The Alfvén layer is defined to be the separatrix

between two sets of drift trajectories, one comprising open drift paths extending from the magnetospheric tail to the dayside magnetopause and another, nearer set consisting of closed drift paths, encircling the Earth [Wolf *et al.*, 2007]. The resistances in the partial ring current and region 2 current, I_2 are R_{prc} and R_{A2} , respectively, and L_2 is the inductance of the region 2 current. The coefficient u_0 in equation (3) is a heat flux limiting parameter. The energy confinement times for the central plasma sheet, parallel kinetic energy and ring current energy are τ_E , τ_k and τ_{rc} , respectively. The effective width of the magnetosphere is L_y and the transition region magnetic field is given by B_{tr} . The pressure gradient driven current is given by $I_{ps} = L_x(p/\mu_0)^{1/2}$, where L_x is the effective length of the magnetotail. The output of the model are the AL and *Dst* indices, in addition to the magnetospheric field aligned currents.

[14] The parameters are combined appropriately into a vector P_d where $d = 18$. They can be estimated using semi analytical techniques or they can be considered as variables that need to be optimized within physically allowable ranges to fit the data for a given storm. The parameters have been approximated analytically using the Tsyganenko magnetic field model and then allowed to vary over a physically reasonable range of values as explained by Spencer *et al.* [2007].

[15] The solar wind dynamo voltage used to drive the model is generated using the Rectified IMF Driver [Reiff and Luhmann, 1986] coupling function ($v_{sw}B_s$) which is given by

$$VB_s = 40(kV) + v_{sw}B_sL_y^{eff}(kV) \quad (9)$$

where v_{sw} is the x-directed component of the solar wind velocity in GSM coordinates, B_s is the southward IMF component and L_y^{eff} is the effective cross-tail width over which the dynamo voltage is produced. For northward or zero IMF B_z , a base viscous voltage of 40 kV is used to drive the system. The rectified $v_{sw}B_s$ was preferred over other coupling functions as it has been shown to be a more robust driver compared to other coupling functions, while maintaining reasonably good feature reproduction capability [Spencer *et al.*, 2009].

[16] The current I_1 used in the model is that portion of the field aligned region 1 current that maps to the nightside central plasma sheet and is considered to be part of the substorm current wedge that produces the westward auroral electrojet. The Auroral AL index now follows as a magnetic field perturbation ΔB_{AL} from the ambient terrestrial field due to the westward electrojet current that flows in the E layer (~ 90 – 120 km) in the nightside ionosphere. We estimate the relation between I_1 and the AL index by assuming that the current I_1 is related linearly to the AL index by a constant of proportionality [Spencer *et al.*, 2007].

[17] The *Dst* signal is obtained from the plasma energy stored in the ring current W_{rc} calculated by the WINDMI model. It is given by the Dessler-Parker-Sckopke (DPS) [Dessler and Parker, 1959; Sckopke, 1966] relation

$$Dst = \frac{\mu_0 W_{rc}(t)}{2\pi B_E R_E^3} \quad (10)$$

where B_E is the Earth's surface magnetic field along the equator.

[18] The ring current energy (W_{rc}) injection terms in the WINDMI model are the first and second terms on the right-hand side of equation (8). The current I_2 is a region 2 current that leaves the ionosphere on the dawnside, closes in the ring current and returns to the ionosphere on the duskside. This secondary loop of current has a self inductance L_2 and drives a current through the partial ring current resistance R_{prc} as well as the resistance of the region 2 current loop footprint R_{A2} . The Joule heating through the resistance R_{prc} energizes the ring current particles. The particles injected across the effective aperture A_{eff} is another source of ring current energy. Equation (8) of the WINDMI model is similar to the *Dst** decay equations of Burton *et al.* [1975] and O'Brien and McPherron [2000]:

$$\frac{dDst^*}{dt} = Q(t) + \frac{Dst^*(t)}{\tau_{rc}} \quad (11)$$

where $Q(t)$ is an injection term and τ_{rc} is the ring current decay rate.

[19] The ring current energy in the model is assumed to be lost by particles drifting out of orbit or by charge exchange processes at a rate proportional to τ_{rc} . It is unclear which of these processes are at work during a particular event. In the model, decay times of around 12 hours indicate that flow out losses dominate, while longer decay times of 18–30 h indicate that charge exchange processes dominate.

3. Optimization With a Genetic Algorithm

[20] The variable coefficients in the WINDMI model are L , M , C , Σ , Ω_{cps} , u_0 , I_c , A_{eff} , B_{tr} , L_y , τ_E , $\tau_{||}$, L_I , C_I , Σ_I , L_2 , R_{prc} , R_{A2} , τ_{rc} , and α . These parameters are constrained to a maximum and a minimum physically realizable and allowable values and combined to form a 18-dimensional search space $S \subset \mathbb{R}^{18}$ over which an optimization is performed.

[21] Genetic Algorithms are general search and optimization methods that are inspired by the concepts of crossover, random mutation and natural selection from evolutionary biology. In the current context, one form of the genetic algorithm [Coley, 2003] is applied to search the physical parameter space in order to minimize the error between the model output and the measured geomagnetic indices. In earlier works with simpler models, the alternate-gradient, steepest-descent, and simulated annealing methods were used to find optimal parameters. These methods were found to have problems getting stuck in local minima. Stochastic search methods such as genetic algorithms perform better in search spaces where objective functions have multiple local minima and are consequently suitable for nonlinear state-space systems such as the WINDMI model.

[22] The optimization scheme was used to select a parameter set for which the outputs from the WINDMI model most closely matches the AL index and the *Dst* index simultaneously. In an earlier work [Spencer *et al.*, 2009] we discussed the results of optimizing against *Dst* only or AL only, or an equal combination of both. For this work we were more interested in the features of the *Dst* index, so we have chosen a higher bias of 0.8 for *Dst* while the AL index was given a weighting of 0.2 in order to maintain a reasonably good fit.

[23] The performance of the algorithm is evaluated by how well the average relative variance (ARV) and correla-

tion coefficient (COR) compare with the measured indices. The average relative variance gives a good measure of how well the optimized model tracks the geomagnetic activity in a normalized mean square sense, while the correlation coefficient shows how well the model tracks the geomagnetic variations above and below its mean value.

[24] The ARV is given by

$$\text{ARV} = \frac{\sum_i (x_i - y_i)^2}{\sum_i (\bar{y} - y_i)^2} \quad (12)$$

where x_i are model values, y_i are the data values, and \bar{y} is the mean of the data values. In order that the model output and the measured data are closely matched, ARV should be closer to zero. A model giving $\text{ARV} = 1$ is equivalent to using the average of the data for the prediction. If $\text{ARV} = 0$, then every $x_i = y_i$. ARV values above 0.8 are considered poor for our purposes. ARV below 0.5 is considered very good, and between 0.5 and 0.7 it is evaluated based upon feature recovery.

[25] The correlation coefficient COR is calculated against the *AL* index only as a measure of performance but not used as a cost function in the optimization process. COR is given by

$$\text{COR} = \frac{\sum_i (x_i - \bar{x})(y_i - \bar{y})}{\sigma_x \sigma_y} \quad (13)$$

COR is better when closer to 1. It indicates anticorrelation if the value is close to -1 . σ_x and σ_y are the model and data variances, respectively. Typically, if the correlation coefficient is above 0.7, the performance is considered satisfactory for the physics based WINDMI model. Both the ARV and COR values are calculated over the period when the most geomagnetic activity occurs.

[26] When these criteria are observed to be acceptable, the optimization process is assumed to have reached convergence. Here we do not explicitly report the ARV or COR values, since we are more interested in the qualitative fit, and the relative contributions from the various current systems.

4. Events and Data

[27] We selected geomagnetic disturbance events in the recent solar cycle that resulted in the *Dst* index dropping off by at least -60 nT (i.e., $Dst < -60$ nT) and for which the IMF B_z was positive (i.e., $v_{sw} B_s = 0$) during the early recovery phase of the storm for relatively long periods of time (at least 12 h). This will turn off the input, $v_{sw} B_s$ into the WINDMI model for some time during the recovery phase so that the initial decay phase is exponential and can be easily analyzed. We note that when there is no energy input, as may occur during an ideal recovery phase of geomagnetic storm, equation (8) has the following simple exponential solution:

$$W_{rc}(t) = W_{rc0} e^{-(t-t_0)/\tau_{rc}} \quad (14)$$

from which one can obtain reasonably accurate values for the decay time τ_{rc} . Storms with relatively long positive IMF B_z conditions during the recovery phase will be termed as having a clean recovery phase.

[28] A total of 13 events have been identified in the period between the years 2000 and 2007, for which the IMF B_z turned northward abruptly after the peak in *Dst* index was observed. Here we use the term “peak in *Dst*” to represent the minimum *Dst* value reached during a storm period since this corresponds to the peak energization level of the ring current particles.

[29] Under the northward IMF turning conditions for the chosen events, the ring current particles are most likely to be trapped and the suggested fast “flow-out” losses on the dayside are probably not significant during the early recovery phase of a storm. Charge exchange losses is then expected to be the dominant mechanism for ring current decay under these conditions. The observed *Dst* decay should then be due to the different charge exchange lifetimes of ions in the ring current and possibly the contributions from other currents in the magnetosphere.

[30] The solar wind parameters in GSM coordinates required as input to the WINDMI model are obtained from the ACE satellite orbiting at the L1 point between the Sun and the Earth. Missing or unusable data from the satellite measurements was dealt with by retaining the previous data value whenever the data was unusable. We discuss this again in section 5. Hourly *AL* and *Dst* index values were obtained from the World Data Center for Geomagnetism, Kyoto Web site.

[31] Most of the events were found during the solar maximum and were caused by coronal mass ejections (CMEs) and flares. Only the event in 2007 (days 81–88) was caused by the passage of a corotating interaction region (CIR) across Earth. The largest storm matching our criteria had a maximum peak in *Dst* of -300 nT, while the smallest storm had an associated *Dst* peak of just -70 nT.

[32] During three of the 13 events the IMF B_z turned northward gradually some time after the peak in *Dst* was observed, but did not change its polarity during the next 12 h. These events were on days 100–104 (2001), 265–268 (2001) and 142–146 (2002). The initial recovery of these three storms could have a more significant contribution from fast flow out losses before charge exchange losses dominate as the IMF B_z turns northward. All 13 events had an associated increase in solar dynamic pressure during the storm main phase. Of the 13 events, six showed an increase in solar wind forcing before complete recovery of *Dst* ($Dst > -20$ nT), as indicated by corresponding increase in $V B_s$ values. These events were on days 158–166 (2000), 260–265 (2000), 100–104 (2001), 80–88 (2002), 245–260 (2002) and 81–88 (2007).

4.1. Decay Times of *Dst* and *Dst** Using WINDMI

[33] One of the outputs of the WINDMI model is the ring current energy which is related to the *Dst* index by the Dessler Parker-Sckopke relation through equation (10). The contribution to the *Dst* index due to the magnetopause currents and other induced currents is not calculated by the model. For this reason it is more appropriate to match the WINDMI *Dst* output against *Dst** which is calculated using the following expression [Kozyra and Liemohn, 2003]:

$$Dst^* = \frac{Dst - Dst_{mp} + D_{grc}}{C_{IC}} \quad (15)$$

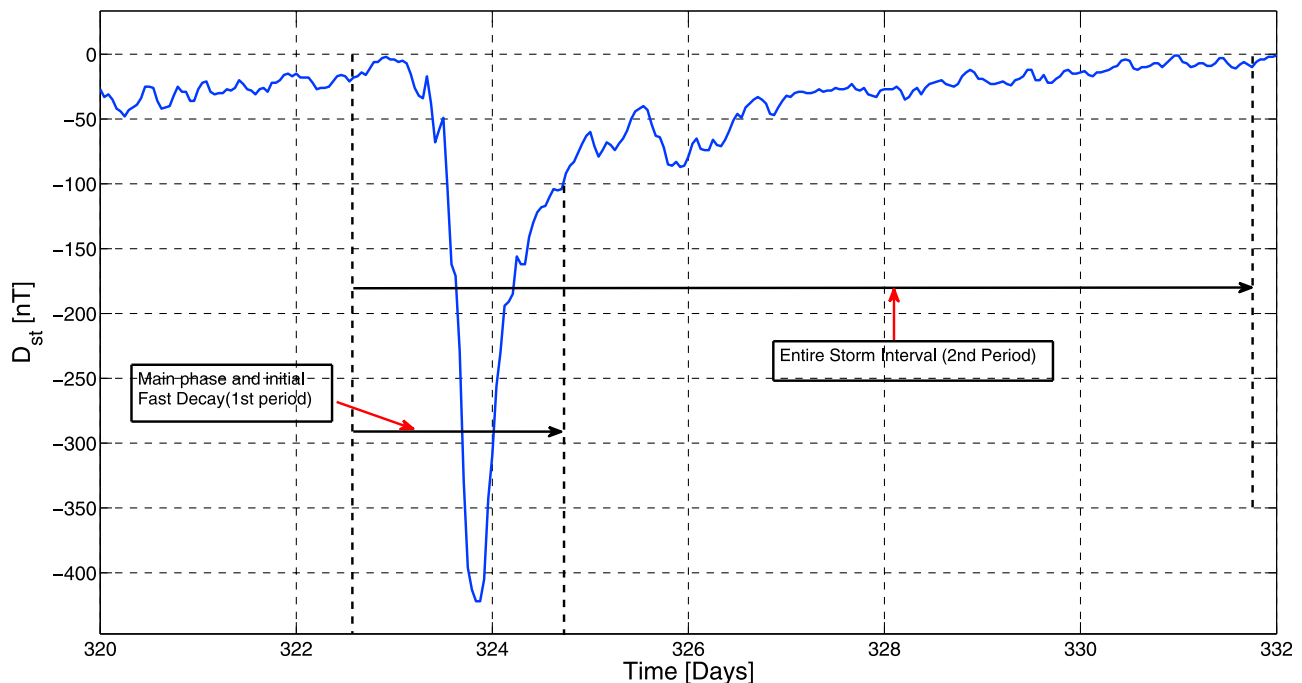


Figure 1. A typical storm time Dst measurement showing the two matching periods used in this work. Period 1 includes the main and the initial fast decay phase, and period 2 is the entire duration of the storm which relates to the overall ring current decay rate.

where C_{IC} is a correction factor due to induced currents in the Earth, which is taken to be 1.3. Dst_{mp} is the perturbation from the Chapman-Ferraro currents on the magnetopause, taken to be $a^* \sqrt{P_{dyn}}$ (solar wind dynamic pressure in nPa), and D_{grc} is the contribution from the quiet time ring current (subtracted out as a baseline offset of the Dst). The factor a is a scaling factor to be explained below.

[34] The WINDMI model does not account for the currents induced on the surface of the conducting Earth due to currents in the magnetosphere. The traditional definition of Dst^* , as mentioned by *Burton et al.* [1975], subtracts the contributions from magnetopause currents and the quiet time Dst values. This definition of Dst^* is the same as the numerator of equation (15). Induced currents flowing inside the Earth's core enhance the measured magnetic field of each external current approximately by C_{IC} . Since the WINDMI model does not model these induced currents, it is more appropriate to divide out this enhancement due to induced currents from the Dst , following equation (15) as mentioned by *Kozyra et al.* [2002]. For this work we have assumed Dst^* to represent the contribution mainly from the ring current and possibly from other magnetospheric currents (other than magnetopause and induced currents).

[35] We used two combination of values for a and D_{grc} . The first one was obtained from *Burton et al.* [1975], and *Kozyra and Liemohn* [2003], and corresponds to values of 15.5 and -20 nT for a and D_{grc} , respectively. The Dst^* obtained using this formula will be henceforth referred to as Dst_B^* in this work. *O'Brien and McPherron* [2000] estimated values of 7.26 for a and 11 nT for D_{grc} , which was the second combination used and the Dst^* calculated with these values will be referred to as Dst_O^* . We therefore obtain two sets of Dst^* values for the 13 selected events.

[36] We optimized the WINDMI model against the AL and Dst indices giving an 0.8:0.2 preference to Dst importance over AL . We mention that it is important to optimize against the AL index with some minimal weighting for all cases because the state variables p , V and I_2 in equation (8) depend on the first seven equations but not vice versa. By including some bias toward AL optimization, the parameters in the first seven equations are constrained consistently.

[37] On the other hand, we want especially to capture the features in the Dst index, so we set a higher bias toward Dst . The higher bias given toward Dst for all our cases makes the parameters in the last two WINDMI equations (7)–(8) have a stronger influence on the results.

[38] Each of the 13 events was optimized twice, once for a period encompassing only the main phase and the initial Dst recovery phase (period 1), and once for the entire duration of the storm (period 2). Recovery of a storm was assumed to be complete after Dst reached values greater than -20 nT. The period selection scheme is illustrated in Figure 1. The scheme was chosen to distinguish between different decay phases of the Dst index during the course of a geomagnetic storm.

[39] This optimization process was repeated for Dst_B^* and Dst_O^* under the same set of criteria as was done for just Dst . Periods 1 and 2 were the same for each event as was estimated for Dst optimization. The optimization results are summarized in Table 1. We make some observations about the selected events and discuss the results of the optimizations in the next section.

4.2. Events and Optimization results

[40] The selected geomagnetic events are discussed in chronological order below. The optimized plots for all the

Table 1. Ring Current Decay Rates Estimated Over Periods 1 and 2 for the 13 Events by Optimizing Against *Dst*, $Dst_{\mathcal{O}}^*$, and Dst_B^* Using the WINDMI Model^a

Event Day	<i>Dst</i> -In	<i>Dst</i> -En	$Dst_{\mathcal{O}}^*$ -In	$Dst_{\mathcal{O}}^*$ -En	Dst_B^* -In	Dst_B^* -En
2000-158	11.1	18.5	10.27	13.57	14.4	24.3
2000-195	16	22.7	15.65	19.35	14.4	26.77
2000-260	16	25.1	11.1	25.9	17.7	42.45
2001-100	5.3	17.7	4.5	14.4	4.5	21
2001-225	16.8	27.6	13.75	16	16.87	42.45
2001-264	15.2	21	14.4	16	21.8	32.55
2001-325	20.1	28.4	20.17	25.95	24.3	48.22
2002-80	14.4	16.1	12.75	13.57	20.1	38.32
2002-142	19.3	33.4	14.4	26.77	15.2	53.17
2002-245	11.9	21.8	11.1	21	13.57	26.77
2004-93	8.6	7.8	7.8	8.62	14.4	16.87
2005-6	16	32.5	16	25.1	12.75	46.57
2007-81	4.5	7.8	5.3	6.97	15.2	38.3

^a*Dst*-In, $Dst_{\mathcal{O}}^*$ -In lists the values for period 1 (initial phase) and *Dst*-En, $Dst_{\mathcal{O}}^*$ -En lists the values for period 2 (entire storm).

events can be found in the auxiliary material.¹ The reason why we discuss the details of each storm event is because we wish to draw attention to similarities and differences between events that might influence the interpretation of the results. Note that *Dst* recovery periods after northward turning of the IMF tend to give more direct and simpler interpretations, based on the discussion earlier.

4.2.1. Days 158–166, 2000

[41] For this event a sudden jump in ACE solar wind velocity and proton density data was observed at 0936 UT on day 159. An associated sudden storm commencement (SSC) was observed in the *Dst* data. The IMF B_z turns northward at 2200 UT on day 160 and stays mostly northward for almost 24 h (up to day 161), following which it turns southward again. Period 1 for this event was from days 158–160.5 in the year 2000. The best WINDMI *Dst* fit to *Dst* data during period 1 yielded a decay time of $\tau_{rc} = 11.1$ h. The entire storm duration which was the same as period 2 for this event was from days 158–164 and the corresponding decay time was $\tau_{rc} = 18.5$ h.

4.2.2. Days 195–202, 2000

[42] This is the extensively studied Bastille day storm that was caused by a solar flare on 14 July 2000. Velocity and proton density data from the ACE satellite were corrupted during the main phase of this event. Around 2000 UT, the IMF B_z at Earth became less negative (increasing to about -10 nT), before turning northward about an hour into 16 July. This effectively ended the convective phase of the storm, and the ring current (as monitored by *Dst* index) began a steady decay during the third hour of the day. The IMF B_z remains mostly northward for a significant duration in the recovery phase (about 48 h).

[43] Due to the prolonged northward IMF period this event shows what we consider as an ideal recovery of *Dst*. The best fits against *Dst* data, for the Bastille day event are shown in Figure 2 corresponding to period 1 of days 195–197.8 and Figure 3 for period 2 comprising the days 195–200. Figures 2 and 3 illustrate the matching technique employed and typical results. From Table 1 it is evident that

an increase in decay under all three matching conditions is observed.

4.2.3. Days 260–265, 2000

[44] Period 1 for this event was from days 260–261.8. Period 2 for this event was from days 260–265. At about 1600 UT on day 260, the *Dst* index showed a positive excursion in value, which corresponds to an associated increase in proton density. The IMF B_z turned southward at 2024 UT on day 260 which triggered the main phase of the storm. The IMF B_z turned northward shortly after the start of day 261 leading to the recovery phase of the event. The best fit values for *Dst* as well as Dst^* show that the WINDMI model ring current estimates a delayed *Dst* minimum as compared to the *Dst* data.

4.2.4. Days 100–105, 2001

[45] This is one of the three events for which the IMF B_z did not turn northward, right after the peak in *Dst* was observed. A 3–5 h delay in attaining the *Dst* minimum was observed in the best fits for all the three indices (*Dst*, $Dst_{\mathcal{O}}^*$, and Dst_B^*). Period 1 for this event was from 100 to 101.5 days, while period 2 was from 100 to 104 days.

4.2.5. Days 225–235, 2001

[46] An SSC event was observed at 1200 UT on day 228, the *Dst* value rose up to almost 50 nT due to this. The IMF B_z turned southward almost immediately signaling the start of the storm. This is another example of a clean event as the IMF B_z turned northward after the peak in the *Dst* index was observed and stayed northward. The recovery was clean as there is no energy input from VB_s , the fluctuation observed in the recovery of the *Dst* index correlate highly with changes in P_{dyn} and is probably due to changing currents in magnetopause.

4.2.6. Days 265–268, 2001

[47] This is the second event for which the IMF B_z turned northward some time after the peak in *Dst* was observed. A significant delay in attaining the *Dst* minimum was observed after finding the best fits for all the three *Dst* indices (*Dst*, $Dst_{\mathcal{O}}^*$ and Dst_B^*). This is one of the smaller storms investigated as indicated by a *Dst* minimum of -70 nT.

4.2.7. Days 325–335, 2001

[48] This event is similar to the Bastille day storm with respect to its recovery phase although it is of lesser intensity. The recovery phase during the long period of northward IMF was clean. ACE solar wind proton and velocity data were corrupted during the storm main phase. Period 1 extends from 327 to 328.5 days and period 2 was taken to be from 327 to 333 days. A clear increase in decay times was observed for the results of best fits for period 1 to period 2 for all three *Dst* indices.

4.2.8. Days 80–88, 2002

[49] The main phase of this twin peaked *Dst* event started at 1424 UT on day 81 when the IMF B_z turned southward. Days 81–84 were assumed to be period 1 and the days from 81 to 8 was taken to be period 2. On days 84–85 during the recovery phase of this event, the IMF B_z turned southward, and the solar wind forcing was large enough to affect the recovery. This activity in the *Dst* index is not predicted by WINDMI, when contribution only from ring current energy is used for matching against *Dst*. Increase in decay from period 1 to period 2 is not evident for *Dst* or $Dst_{\mathcal{O}}^*$, but for Dst_B^* a clear increase in decay time is observed. The optimized results for this event are shown in Figures 4–9.

¹Auxiliary materials are available in the HTML. doi:10.1029/2010JA015824.

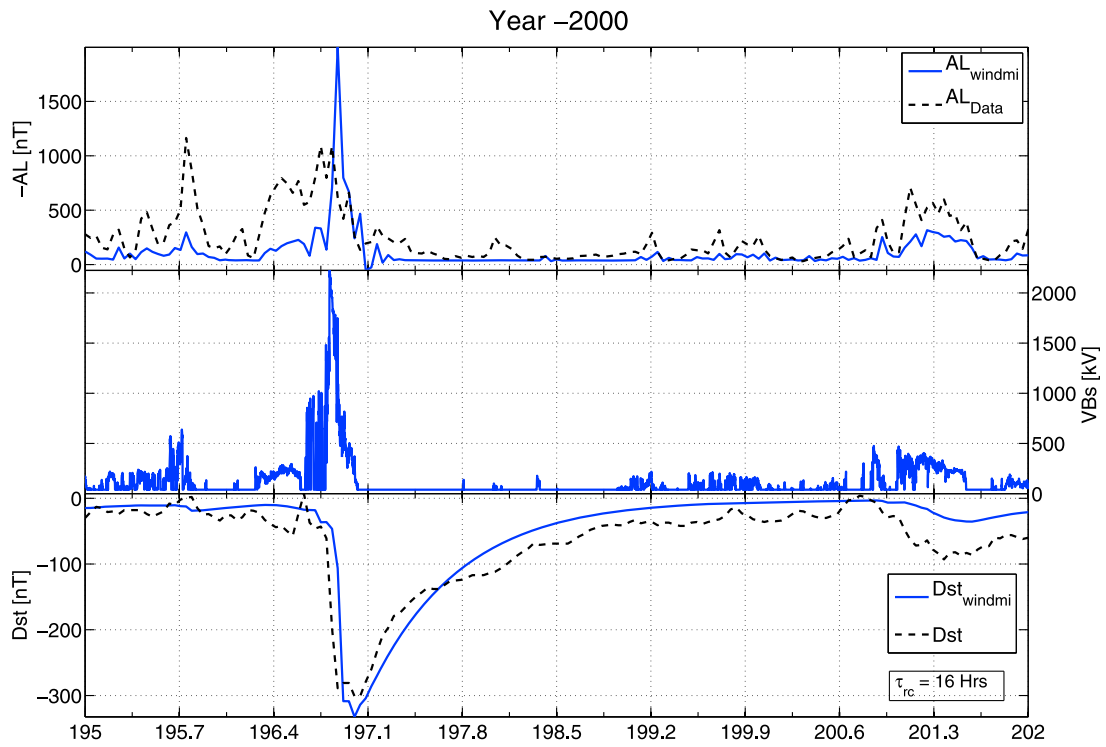


Figure 2. The best fit for days 195–197.8 (main and early recovery phase, period 1) of the event (195–200 days) in the year 2000, obtained by optimizing with a $0.8 \cdot Dst : 0.2 \cdot AL$ preference to measured data.

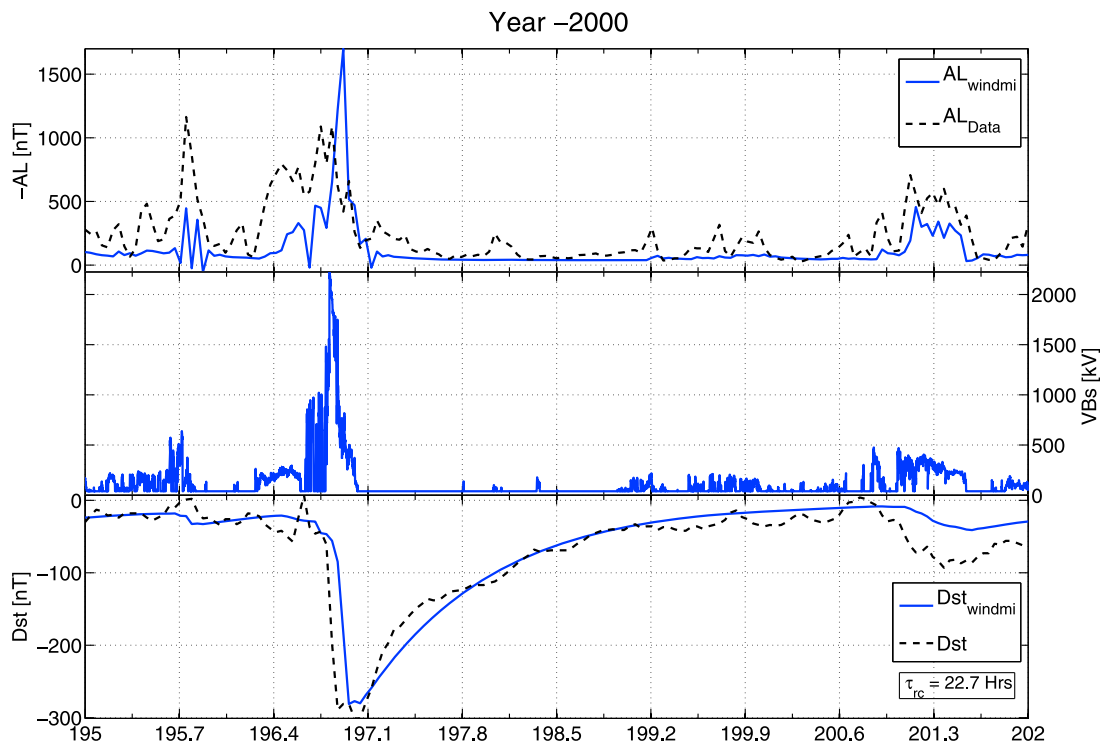


Figure 3. The best fit for the event on days 195–200 (entire storm, period 2) in the year 2000, obtained by optimizing with a $0.8 \cdot Dst : 2 \cdot AL$ preference to measured data.

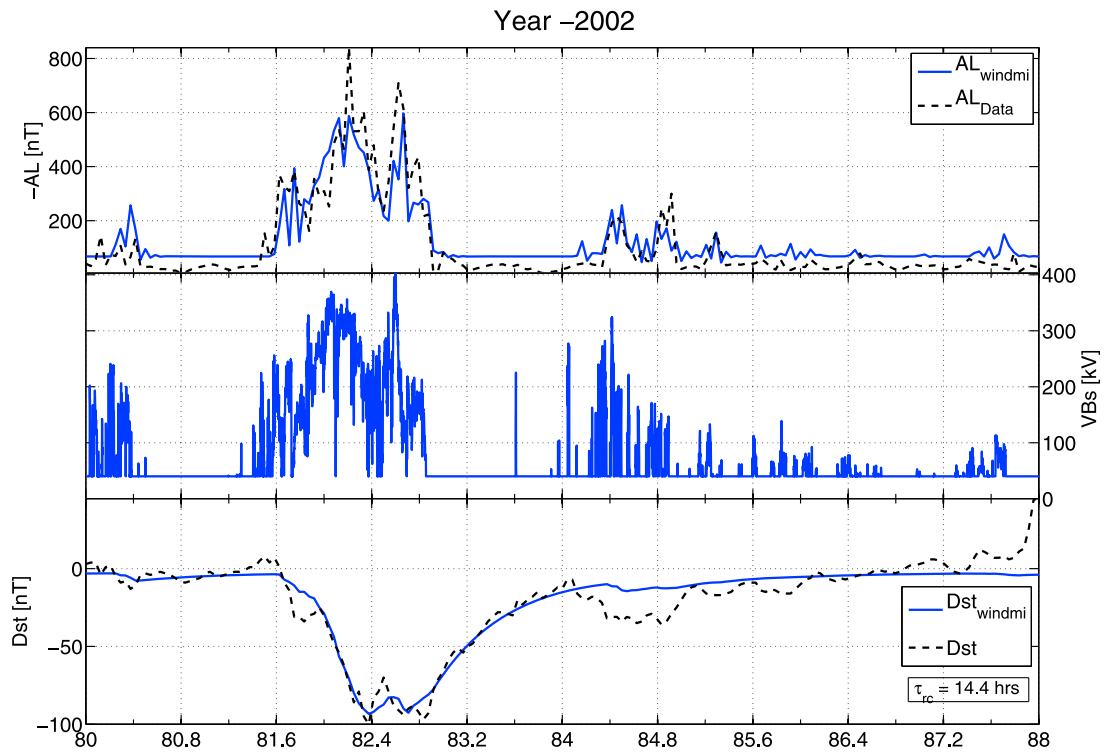


Figure 4. The best fit for days 81–84 (main and early recovery phase) of the event on (days 81–87) in the year 2002, obtained by optimizing with a $0.8 \cdot Dst : 2 \cdot AL$ preference to measured *Dst* data.

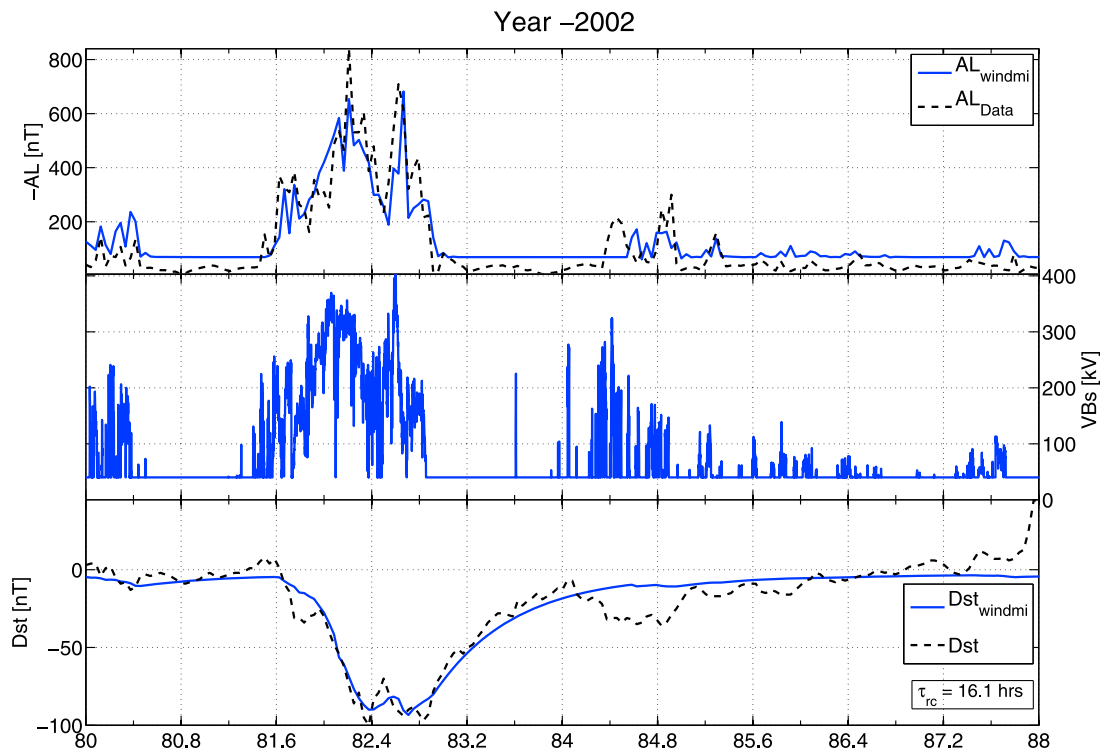


Figure 5. The best fit for the event of days 81–87 (entire storm) in the year 2002, obtained by optimizing with a $0.8 \cdot Dst : 0.2 \cdot AL$ preference to measured *Dst* data.

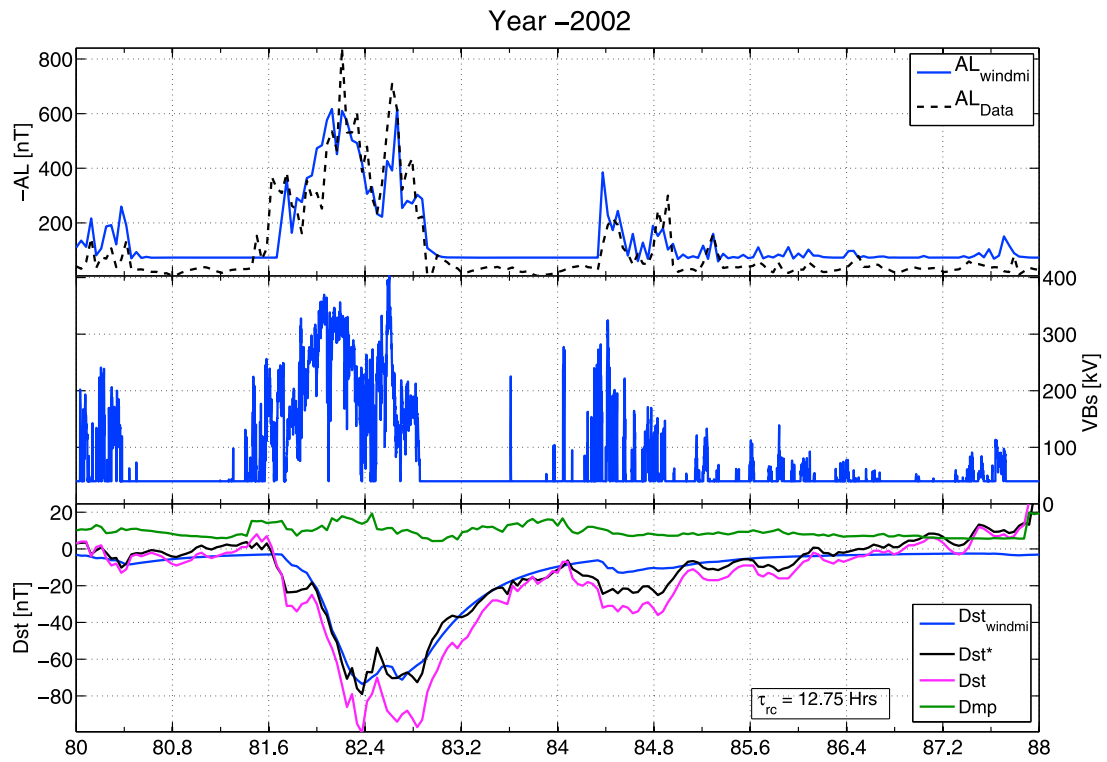


Figure 6. The best fit for days 81–84 (main and early recovery phase) of the event on (days 81–87) in the year 2002, obtained by optimizing with a $0.8 \cdot Dst : 2 \cdot AL$ preference to $Dst \cdot O$ data.

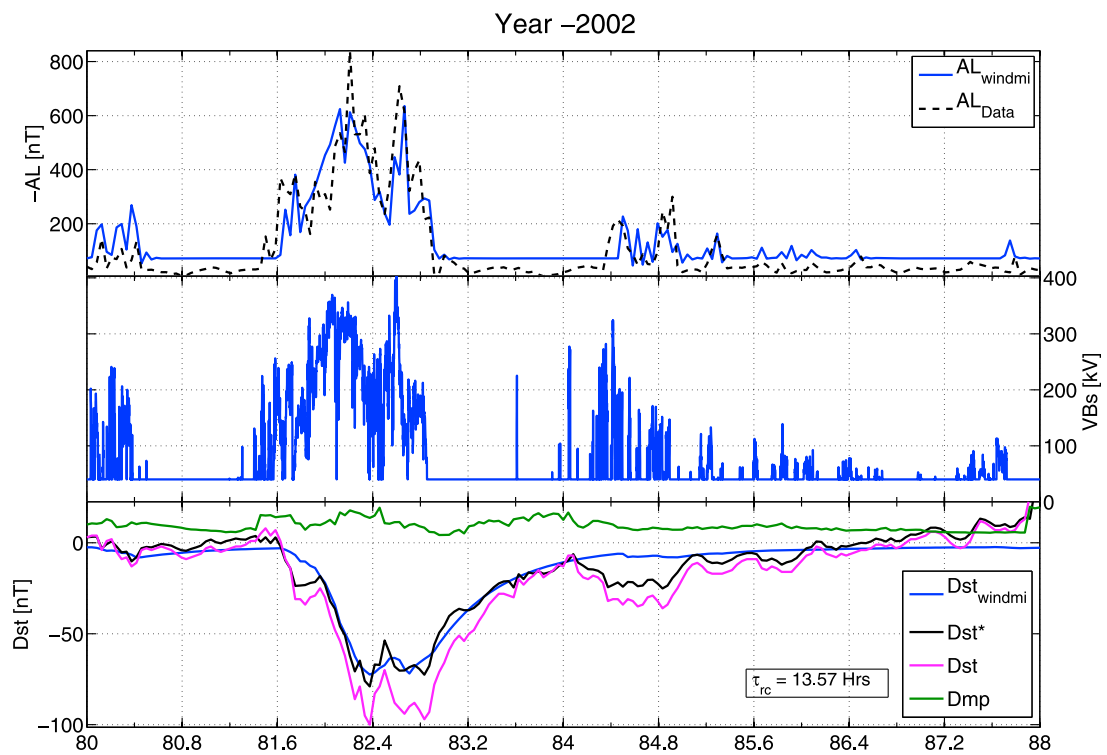


Figure 7. The best fit for the event of days 81–87 (entire storm) in the year 2002, obtained by optimizing with a $0.8 \cdot Dst : 0.2 \cdot AL$ preference to measured $Dst \cdot O$ data.

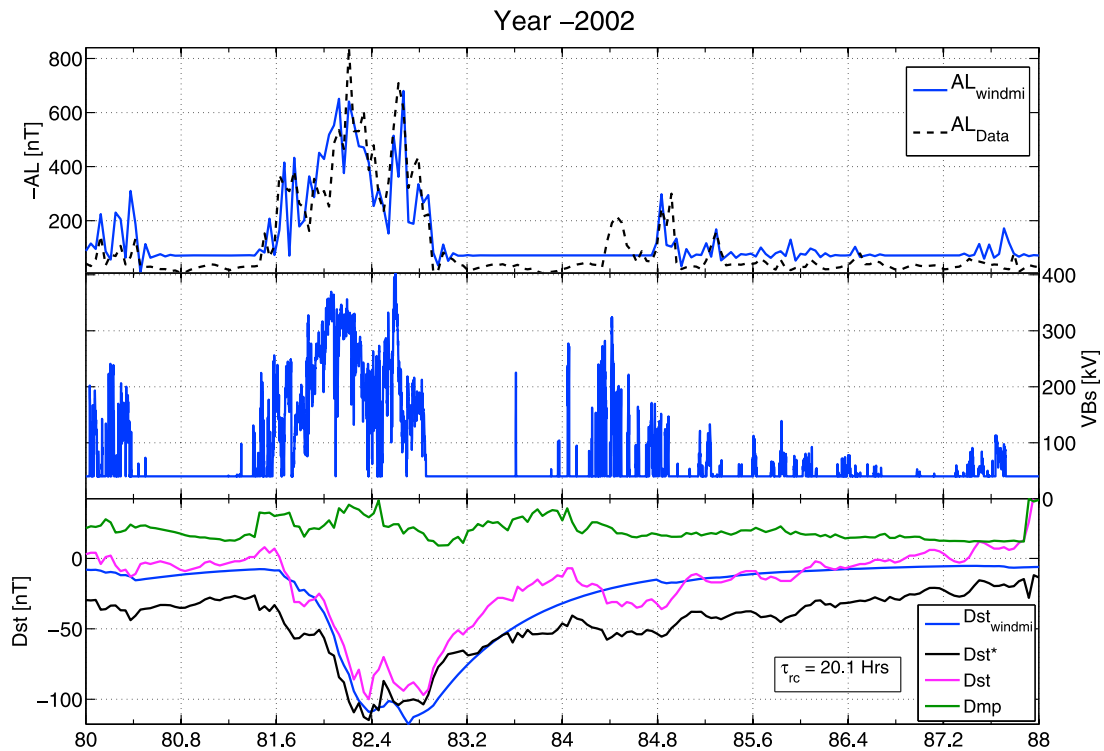


Figure 8. The best fit for days 81–84 (main and early recovery phase) of the event on (days 81–87) in the year 2002, obtained by optimizing with a $0.8 \cdot Dst : 2 \cdot AL$ preference to $Dst \cdot B$ data.

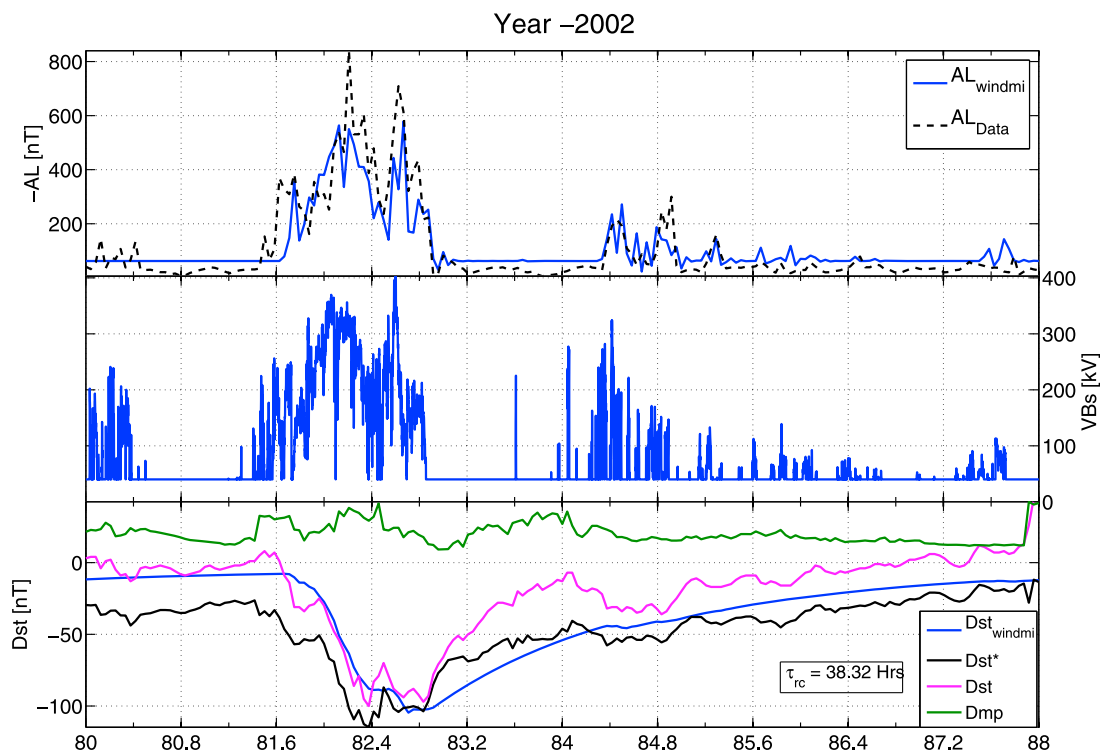


Figure 9. The best fit for the event of days 81–87 (entire storm) in the year 2002, obtained by optimizing with a $0.8 \cdot Dst : 0.2 \cdot AL$ preference to measured $Dst \cdot B$ data.

[50] Pressure enhancements during the recovery phase of the Dst index probably had a role to play in the faster recovery of the measured Dst . The contributions of magnetopause currents to the measured Dst are higher according to the values of *Burton et al.* [1975] compared to the numbers suggested by *O'Brien and McPherron* [2000]. This difference can be seen in the Dst_B^* and Dst_O^* plots shown in Figures 6, 7, 8, and 9.

4.2.9. Days 142–146, 2002

[51] This is the third event of the 13 events for which the IMF B_z turned northward 9.6 h after the peak in Dst was observed. The storm duration was relatively short compared to the other events. The SSC at the start of the main phase of this event resulted in Dst reaching values higher than +50 nT. The plots for Dst_O^* and Dst_B^* which are included in the auxiliary material, show significant differences in accounting for the SSC effects. Dst_O^* estimates the contribution of pressure enhancements to be lower and hence still shows large positive excursion in its values. The larger contribution of P_{dyn} to Dst_B^* ensures that the resulting values remain negative.

4.2.10. Days 245–260, 2002

[52] This was a multistage event. The first stage had an SSC associated with it. The IMF B_z turned northward for a short while after the peak in Dst for the second and the largest event. The IMF B_z was again southward during the recovery phase while the Dst recovered to its quiet time values. The optimization ranges are short compared to the total event duration. Period 1 is from 249 to 251, while period 2 is from 249 to 252. The increase in decay time observed is obtained during the period of northward IMF B_z in the recovery phase.

4.2.11. Days 93–95.5, 2004

[53] This is one of the shortest duration events that we analyzed, lasting only 3 days. The Dst recovered from its peak value to a value of -20 nT within just one and a half days. The event on days 93–95.5 (2004) was followed by increased solar wind forcing as the IMF B_z again changed direction to become southward on day 95.5, thus complete deenergization of ring current particles may not have occurred. Increase in P_{dyn} during the recovery phase also affected the recovery rates.

4.2.12. Days 6–10, 2005

[54] During the storm main phase, ACE proton density values were missing. The IMF B_z was mostly northward for almost the complete duration of the storm recovery. Again an increase in decay times from period 1 to 2 is observed for all the three indices.

4.2.13. Days 81–88, 2007

[55] On days 81–88 (2007), the IMF B_z turned northward for a short duration during a CIR event while the rest of the time the IMF B_z fluctuated between two polarities. P_{dyn} enhancement during the period of northward B_z is the dominant contributor to Dst recovery in this case. The increase in τ_{rc} observed by optimizing against both Dst and Dst^* for this case is because of continuous injection of energy from the solar wind as B_z fluctuates, resulting in an increased effective decay time. Noticeable differences can be found in the Dst_O^* and Dst_B^* plots, which we discuss below.

4.3. Two-Phase Decay Observations

[56] From Table 1, we observe that for most of the cases an increase in the decay period of Dst indices are obtained,

from optimizing the model during period 1 compared to period 2. However, for the events on days 80–88 (2002), 93–95.5 (2004), and days 81–88 (2007), an almost insignificant difference was obtained.

[57] Matching results using Dst_B^* for the event on days 80–88 (2002) show an increase in decay time from period 1 to period 2, which was not evident for Dst and Dst_O^* . The decay times optimized for period 2 of Dst_B^* is consistently higher compared to Dst and Dst_O^* values.

[58] From Table 1 we notice that the event in 2004 is the only event for which a clear increase in decay time for the entire storm duration is not observed. All three best fits against Dst , Dst_O^* and Dst_B^* data for this event show only a marginal increase in decay times.

[59] Using Dst_B^* for the event on days 81–88 (2007) shows that the increase in decay times is because of CIR induced IMF B_z fluctuations. The higher contribution of pressure enhancements effects in Dst_B^* almost completely removes the fast decay during the period of northward IMF for this event. This is in contrast to the results obtained using Dst and Dst_O^* , which are significantly affected by the sharp recovery due to P_{dyn} .

[60] It should be noted that the τ_{rc} numbers estimated by the WINDMI model by optimizing against Dst are not true representations of the recovery of ring current particles. Contributions from magnetopause currents due to pressure enhancements and other magnetospheric currents affect the decay rates. Using pressure corrected Dst^* does not completely resolve this issue, as the relative contribution of Dst_{mp} is not accurately known yet. However, these values are a more accurate representation of the contribution of the near-Earth current systems.

[61] The increase in decay times observed agree with the findings of *O'Brien et al.* [2002], who show that storms with abrupt northward turning of IMF B_z show the same amount of recovery in the first 6 hours or slightly faster recovery than do the storms with gradual northward turnings. This could be attributed to a gradual increase in decay times of ring current particles or a manifestation of the recovery times of the other magnetospheric current systems. The tail current in particular, is known to decay on a much smaller timescale compared to the ring current.

[62] In section 5 we describe how the inclusion of the tail current and magnetopause currents influences the observed decay rates.

5. Contribution of Magnetospheric Currents

[63] The major current systems in the magnetosphere are (1) the magnetopause currents shielding Earth's dipolar magnetic field, (2) the symmetric ring current, (3) the partial ring current, and (4) the cross-tail current along with the closure currents on the magnetopause. All these currents cause magnetic perturbations on the Earth's surface. The results in the last section indicate that there is an increase in decay times as the Dst recovers during a magnetic storm even under abrupt northward turning of IMF B_z . To contrast the contribution of other currents to this observation, we add the magnetopause current and cross-tail current contributions in addition to the WINDMI ring current in order to calculate the simulated Dst index. The quiet time values for

Table 2. Ring Current Decay Rates Obtained After Including the Effects of Magnetopause and Tail Current Contributions to *Dst* Simulated by WINDMI^a

Event Day	τ_{rc} Burt (in h)	τ_{rc} O'Brien (in h)
2000-158	26.0	21.4
2000-195	39.8	31.5
2000-260	43.4	34.27
2001-100	40.7	26.92
2001-225	33.4	23.25
2001-264	30.6	26.0
2001-325	37.9	33.35
2002-80	40.7	25.0
2002-142	54.4	38.86
2002-245	39.8	36.1
2004-93	22.3	14
2005-6	54.48	36.11
2007-81	34.3	24.16

^aHere τ_{rc} Burt stands for the ring current decay rates obtained using Burton *et al.*'s [1975] formula for Dst_{mp} ; τ_{rc} O'Brien are the result using O'Brien and McPherron's [2000] values for Dst_{mp} .

each current system is included in the WINDMI model calculations.

[64] Liemohn *et al.* [2001] obtained the contribution of the partial ring current (PRC) to *Dst* during the storm main phase to be as large as 80%. Maltsev [2004] estimate the contribution of the PRC with the induction currents inside the Earth to be 15%. They argue that neglecting the polarization electric field originating from charge separation in the course of particle sunward convection led to the substantially higher values obtained by Liemohn *et al.* [2001]. According to Tsyganenko and Sitnov [2005] the westward near-equatorial part of the PRC is largely offset in the dawn sector by the opposite effect of the field-aligned closure currents, hence their contribution to the *Dst* is very small compared to the ring current and tail current contributions. WINDMI models the PRC as flowing partially in the ring current and closing through the region 2 current I_2 (refer to equation (7)). In the model, the timescale and dynamics of the I_2 current are very close to the timescale and dynamics of the geotail current I . Here we have lumped together the effects of the region one and two currents, I_1 , I_2 , and the geotail current and proceed to use αI of the geotail current to represent both. The contributions from the magnetopause and tail current systems are given by

$$Dst_{mp} = a^* \sqrt{P_{dyn}} \quad (16)$$

$$Dst_t = \alpha I(t) \quad (17)$$

where Dst_{mp} is the perturbation due to the magnetopause currents and Dst_t is the magnetic field contribution from the tail current $I(t)$ which is modeled by WINDMI as I . P_{dyn} is the dynamic pressure exerted by the solar wind on the Earth's magnetopause. We used two values 15.5 and 7.26 for a as estimated by Burton *et al.* [1975] and O'Brien and McPherron [2000], respectively. Burton's formula estimates the contribution of Dst_{mp} to be more than twice that estimated by O'Brien's formula. The factor α is an unknown geometrical factor that is optimized, and accounts for the

errors introduced due to the assumed structure of the geotail. The simulated *Dst* is then given by

$$Dst_{windmi} = Dst_{rc} + Dst_{mp} + Dst_t \quad (18)$$

Using expression (18) to calculate the simulated *Dst*, we optimized the physical parameters of the WINDMI model and the geometrical factor α for all the events again. The optimized ring current decay periods are compared against the results from section 4.1. We obtain two set of results one each for the two values of a .

[65] Estimates for the value of α can be inferred from calculations similar to as given by Kamide and Chian [2007, pp. 364–365], but we chose to make it an optimization variable here. We optimized the value of α for the event that occurred on days 325–335 in the year 2001. The best fit value was found to be 4.3 per MA . This value of α was then kept fixed for all the other events. Kamide and Chian [2007] estimated that, assuming the PRC and near-Earth cross-tail currents are confined within 18 to 06 local time sector in the nightside, at a distance of $6 R_E$, each MA of the combined currents produce a disturbance of 10.4 nT on the Earth's surface at low latitudes. Since the effects of the individual currents are unclear, we leave a comparison of our values of α with the values found by Kamide and Chian [2007] for future work.

5.1. Results After Including Magnetopause and Tail Current Contributions

[66] Following the procedure that we used in reporting our results in subsection 4, we discuss all the 13 individual events again but now using the results from the modified *Dst* formula. The ring current decay times τ_{rc} estimated after including the contributions from other magnetospheric currents for all the events for both the Dst_{mp} values is compiled in Table 2. All the 26 plots generated and discussed in this section have been included in the auxiliary material.

5.1.1. Days 158–166, 2000

[67] Addition of contributions from the magnetopause currents now allow the modeled *Dst* to predict the SSC at the start of this event. During the medium activity following the period of northward decay, optimization results using O'Brien's formula for Dst_{mp} fit the data better compared to those using Burton's formula. The best fit using the modified *Dst* formula yields decay times of 26 h using Burton's formula and 21.4 h using O'Brien's formula. Any positive deflections for the estimated *Dst* values is only due to contributions from Dst_{mp} , since tail current $I(t)$ and ring current (represented by W_{rc}) weaken the Earth's magnetic field and are negative contributions in the model. The SSC is slightly under predicted by O'Brien's formula while it is over predicted by Burton's formula.

5.1.2. Days 195–202, 2000

[68] For the Bastille day storm, during the storm main phase the contribution from the tail current to the *Dst* exceeds that of the ring current for both the formulas. The ring current seems to take a longer time to energize and also decays on a much longer timescale. Figure 10 shows the Bastille day event optimized using Burton's formula for Dst_{mp} contribution. Possible errors in the results due

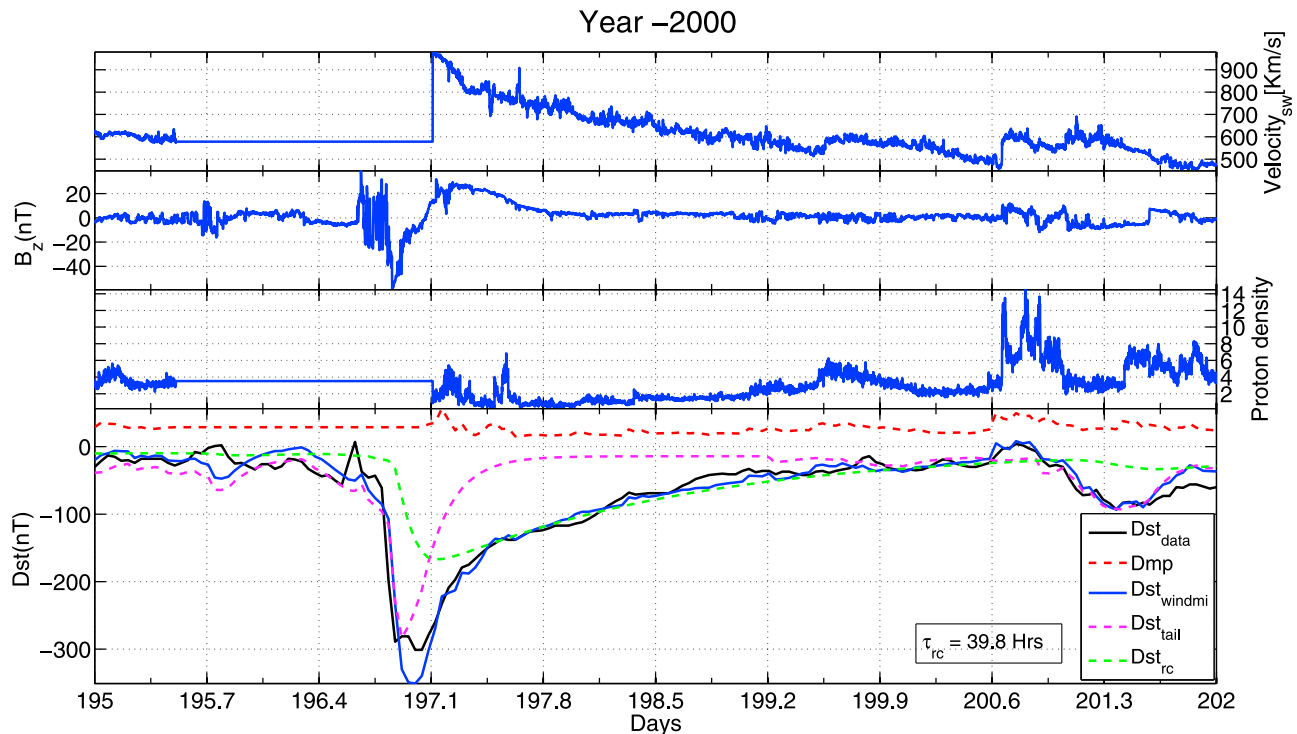


Figure 10. Modeled results using the modified WINDMI Dst formula for the storm that occurred on days 195–200 in the year 2000. Colored lines correspond to individual contributions to the storm time Dst from the major currents in the magnetosphere. Burton’s formula was used to estimate Dst_{mp} .

to missing or unusable data is highlighted in this event. Solar wind proton density and velocity data as measured by ACE was missing during the main phase of this storm. We retained the previous data value for all the solar wind measurements that are either missing or corrupted. The Dst_{mp} values during the initial and main phase are probably underestimated due to our choice of data reconstruction, as the quiet time values are generally smaller. This leads to the over estimation of the Dst peak value as can be seen in the Figure 10.

5.1.3. Days 260–265, 2000

[69] As described earlier, optimizing using just the ring current contribution from the WINDMI model against Dst data resulted in the delayed prediction of the Dst peak location. The faster dynamics of the tail current help the modified Dst optimized results to predict the rise and peak location of the Dst more accurately. The tail current also helps in capturing the moderate activity during days 262–263.

5.1.4. Days 100–105, 2001

[70] The main phase is not that well reproduced by the modified Dst for the first event in 2001. The faster decay time of the tail current helps the modified Dst formula in predicting the minimum in Dst earlier than what was possible with just Dst from the WINDMI ring current. This was one of the events for which the IMF B_z did not turn northward abruptly after the peak in Dst . The results for the main phase suggest that there are probably more physical processes which still need to be accounted for to get a more realistic representation.

5.1.5. Days 225–235, 2001

[71] The simulated results for the event is shown in Figure 11. Burton’s formula was used in estimating Dst_{mp} for Figure 11. Several improvements over the previous model can be immediately observed. The sudden storm commencement due to the initial pressure enhancement caused by the shock front is reproduced. Minor variations in Dst index are now better predicted as the contribution from faster recovering tail currents and P_{dyn} are included. IMF B_z was northward for a long time for this event and changes in the Dst_{mp} are well correlated with fluctuations in the recovery phase. The model over predicts the Dst peak by -40 nT using Burton’s formula. The ring current recovery time τ_{rc} is predicted to be 33.4 h, which is significantly higher than the 16.5 h estimated for the same event by matching against Dst for period 1 (refer to Table 1). The induced disturbance due to the ring current is predicted to be a lot higher in this case, but is compensated by the associated increase in magnetopause currents due to pressure enhancements.

[72] Using O’Brien’s formula for this event the model under predicts the SSC before the start of the main phase. But it does not over predict the value of minimum Dst . The ring current recovery time for O’Brien’s formula is 23.25 h, which is less than what was predicted using Burton’s formula, but still substantially higher than that predicted by matching during period 1 for all the Dst indices shown in Table 1. The modified Dst for this case captures the moderate event on days 232–234.

5.1.6. Days 265–268, 2001

[73] The best fits for this event as discussed in section 4 showed that the WINDMI model predicts a delay in the

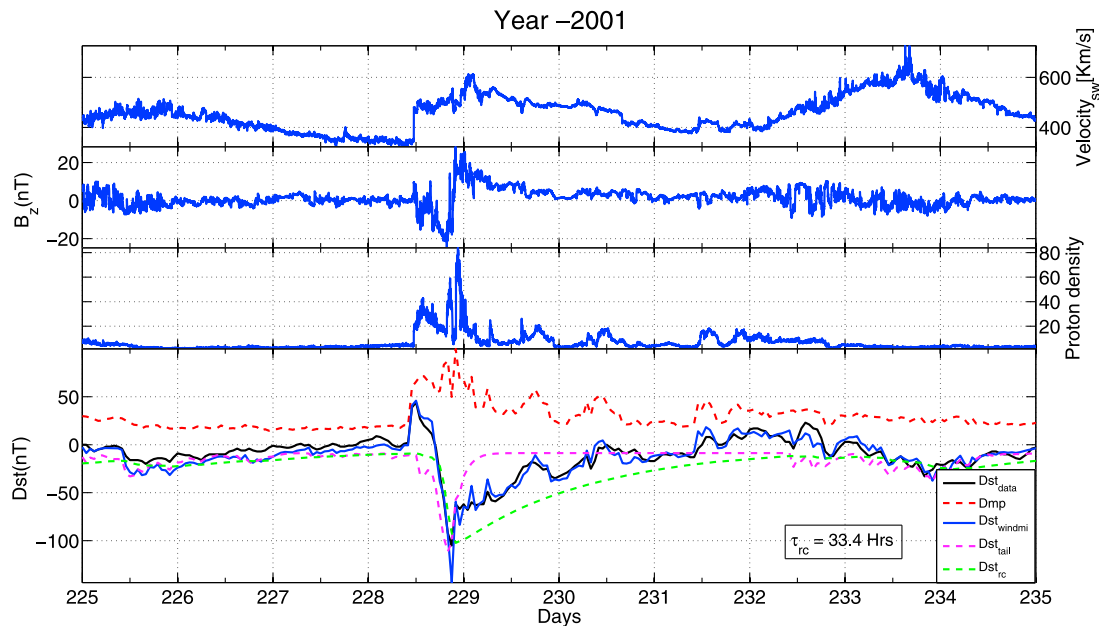


Figure 11. The best fit for the storm that occurred on days 228–233 in the year 2001 obtained using the modified model. Colored lines correspond to individual contributions to the storm time Dst from the major currents in the magnetosphere. Burton’s formula was used to estimate Dst_{mp} .

Dst peak location. The modified Dst formula now predicts a peak location which is much closer to measured data. This is another event where the faster dynamics of the tail current helps in predicting the Dst minimum earlier and closer to the measured Dst , than was possible with just Dst from WINDMI ring current energy.

5.1.7. Days 80–88, 2002

[74] In section 4.1 we discuss that for the event on days 80–88 (2002), the effect of increased solar wind forcing observed on day 84 was not properly predicted by the optimized Dst results. Pressure enhancements during the recovery phase of the Dst index helped in the faster recovery of the measured Dst . The modified model result using Burton’s coefficient for Dst_{mp} for this event is shown in Figure 12. The modeled values suggest that the ring current particles lost energy on a much longer timescale as indicated by the effective τ_{rc} value of 40.7 h. Complete deenergization of the ring current particles was not possible before the moderate storm, which is now fairly well reproduced.

[75] With the modified Dst using Burton’s formula we are able to obtain the moderate event on day 84. Using O’Brien’s formula the results for the main phase and early recovery phase of the storm are good but the ring current recovers a lot faster and is not able to capture this drop in Dst during the recovery phase as the ring current appears to have deenergized completely when using O’Brien’s formula.

5.1.8. Days 142–146, 2002

[76] This was the third event with a gradual northward turning of the IMF B_z . The ring current takes much longer to decay compared to the tail current. The best fit using Burton’s formula for Dst_{mp} suggests a longer decay time for the ring current. The different contributions of P_{dyn} as estimated by Burton and O’Brien can now be seen to affect

the SSC at the start of this storm. Both the formulas under predict the SSC but Burton’s values are closer to data while contributions from O’Brien’s values barely show positive values of Dst .

5.1.9. Days 245–260, 2002

[77] This multistage event had an associated SSC at the start of the storm. Using Burton’s formula for Dst_{mp} , the SSC is captured but not with O’Brien’s. Ring current recovers on a much longer timescale. The duration of this event was from days 245 to 260. The period of northward IMF was only during the initial recovery phase of the second and largest peak in Dst between days 249 and 250.

5.1.10. Days 93–95.5, 2004

[78] The fast decay of the tail current helps in predicting both the main event and second event following the storm. The ring current decay times predicted are smaller especially for Dst_{windmi} with O’Brien’s formula for this particular event.

5.1.11. Days 6–10, 2005

[79] This is one of the smallest events that we have analyzed. Due to missing solar wind proton density data during the storm main phase, the contribution of Dst_{mp} is probably underestimated. The modified Dst values significantly over predict the Dst values during the main phase of the storm as well as the minimum in Dst . The decay period is modeled well.

5.1.12. Days 81–88, 2007

[80] This was the only CIR event that matched our criterion in the period under consideration. In section 4.3, where we discuss the increase in decay times from the best fits for Dst and Dst^* , we expected that the fast decay during the period of northward IMF during the recovery phase was probably due to pressure enhancement and not actual ring current recovery.

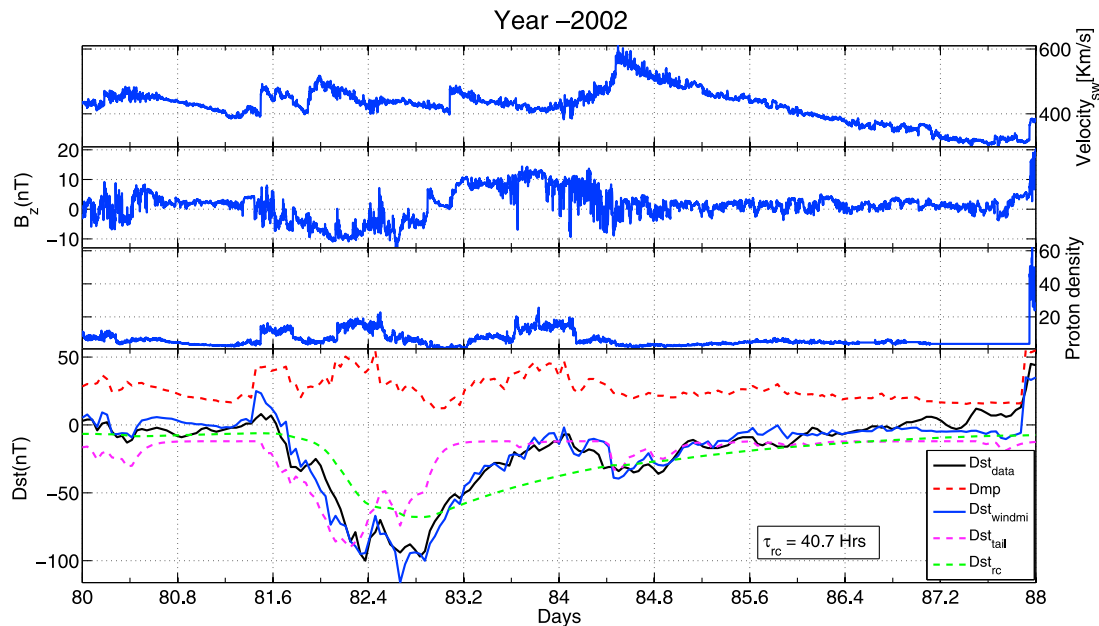


Figure 12. Modeled Dst results for a storm that occurred on days 80–88, 2002 using the modified WINDMI Dst expression. Colored lines correspond to individual contributions to the storm time Dst from the major currents in the magnetosphere. Burton’s formula was used to estimate Dst_{mp} .

[81] The results in this section indicate that the variation can be accounted for by the faster timescale Dst_{mp} and tail current dynamics. The ring current decay times predicted are 34.13 h and 24.16 h for Burton’s and O’Brien’s formulas, respectively. Using O’Brien’s formula we are not able to get the positive excursions of the Dst index during the initial recovery phase from 82.7 to 83.2 days. Proton density data were lost during the start of the storm and the probable underestimation of Dst_{mp} during that period probably causes under prediction of Dst values over that period.

5.2. Discussion

[82] The results compiled in Table 2 suggest that the ring current may decay on a much longer timescales than previously estimated. Contributions from the tail current combined with contributions from other fast ring current decay mechanisms can account for the initial fast decay of the Dst index. For all cases, using O’Brien’s formula for estimating Dst_{mp} gave us values for τ_{rc} which were less compared to using Burton’s formula.

[83] The errors in the modeled Dst can be expected to increase during events when southward IMF B_z slowly turns northward, as the fast decay of Dst is due to both the tail current recovery as well as the flow out loss of particles from the ring current during B_z south. In addition it has been reported that when the component of the E_y due to VB_s is large, the ram pressure contribution to Dst might decrease [Siscoe et al., 2005], leading to a greater variation in our results.

[84] To test the performance of the model we use an out of sample event, a strong storm that occurred between 6 and 10 April 2000 with a peak Dst of -300 nT. The IMF B_z turns northward abruptly after the peak in Dst is observed, but only for a short duration after which it turns southward again

and gradually fluctuates to its quiet time values. The optimized WINDMI results for this event are shown in Figure 13. This event was studied in detail by Tsyganenko and Sitnov [2005], who included contributions from all the major magnetospheric systems in estimating their Dst index. They report symmetric ring current and tail current decay times that are similar to our results. The tail current contributions as estimated by WINDMI during the main phase of this storm exceeds that of the ring current which agrees with their findings.

[85] Our results for this out of sample event, suggest significantly higher values for both ring current and tail current contribution to Dst for this event, as compared to the results of Tsyganenko and Sitnov [2005]. The higher estimate could be due to the faster ring current decay mechanisms which are not included in our model, may have a major role to play during the early recovery phase of the storm. Since the decay rates of the tail current and these faster mechanisms are approximately on the same timescale, the optimization algorithm boosts the tail current contributions to compensate for the absence of other effects.

6. Conclusion

[86] In this work we analyzed 13 events in the recent solar cycle where the IMF B_z was northward during the early recovery phase of the storm. We separated our investigation into two parts, first we tested to confirm whether a two phase decay is evident even for abrupt northward IMF turning cases, and second, we included contributions from different magnetospheric current systems to the measured Dst index. The analysis indicates that the two phase decay is evident even after abrupt northward turning of IMF B_z during the storm recovery phase. This result agrees with the

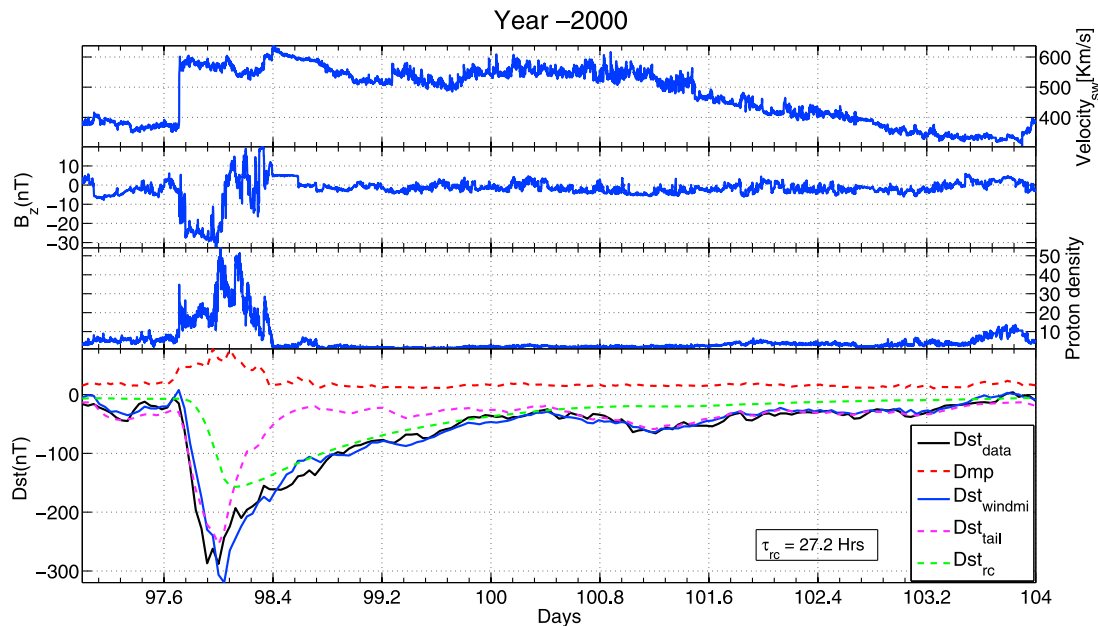


Figure 13. Modeled Dst results for a storm that occurred on 6–10 April 2000. IMF B_z was not northward for any significant length of time during the early recovery phase of this storm. Burton's formula was used to estimate Dst_{mp} .

findings of O'Brien *et al.* [2002], who also observed a similar recovery trend for both northward and southward B_z cases.

[87] We used two different formulas for estimating the pressure corrected Dst^* , one due to O'Brien and the other using Burton's coefficients. The two contributions for Dst_{mp} were also included in calculating the total contribution from the magnetospheric currents to the Dst index. Optimization with the two different formulas for the modified Dst gives mixed results as far as the extent of the contributions from Dst_{mp} is concerned. The optimization algorithm chooses the amount of contribution from each component in order to get a best fit to the total Dst . At this time we cannot conclude whether one formula should be preferred over the other.

[88] The storm-time dynamics of individual contributions of principal external field sources to the ground magnetic disturbance is modeled well by including the contributions from magnetopause and tail currents in the WINDMI model. Our results support the findings of Alexeev *et al.* [1996, 2001], Maltsev *et al.* [1996], and Tsyganenko and Sitnov [2005], who report that the tail current and the ring current dynamics are the most important contributors to the Dst index. In most cases, the tail field even exceeds the contribution due to the ring current during the main phase, but then quickly subsides, leaving the symmetrical ring current as the dominant source through the rest of the recovery phase. The modeled results indicate longer decay times for the symmetric ring current.

[89] The WINDMI model can be improved further by accounting for the different loss processes of the ring current particles by making τ_{rc} a function of the factors affecting the individual loss processes. Results obtained in this paper were made under the assumption that particles are trapped on closed field lines when the IMF B_z becomes northward.

[90] **Acknowledgments.** This work was partially supported under NSF grant NSF-0720201. The solar wind plasma and magnetic field data were obtained from ACE instrument data at the NASA CDA Web site. The geomagnetic indices used were obtained from the World Data Center for Geomagnetism in Kyoto, Japan.

[91] Masaki Fujimoto thanks the reviewers for their assistance in evaluating this paper.

References

- Alexeev, I. I., E. S. Belenkaya, V. V. Kalegaev, Y. I. Feldstein, and A. Grafe (1996), Magnetic storms and magnetotail currents, *J. Geophys. Res.*, *101*(A4), 7737–7747, doi:10.1029/95JA03509.
- Alexeev, I. I., V. V. Kalegaev, E. S. Belenkaya, S. Y. Bobrovnikov, Y. I. Feldstein, and L. I. Gromova (2001), Dynamic model of the magnetosphere: Case study for January 9–12, 1997, *J. Geophys. Res.*, *106*(A11), 25,683–25,693, doi:10.1029/2001JA900057.
- Burton, R. K., R. L. McPherron, and C. T. Russell (1975), An empirical relationship between interplanetary conditions and Dst , *J. Geophys. Res.*, *80*(31), 4204–4214, doi:10.1029/JA080i031p04204.
- Coley, D. A. (2003), *An Introduction to Genetic Algorithms for Scientists and Engineers*, World Sci, Tokyo.
- Daglis, I. A., R. M. Thorne, W. Baumjohann, and S. Orsini (1999), The terrestrial ring current: Origin, formation, and decay, *Rev. Geophys.*, *37*(4), 407–438, doi:10.1029/1999RG900009.
- Dessler, A., and E. N. Parker (1959), Hydromagnetic theory of geomagnetic storms, *J. Geophys. Res.*, *64*, 2239–2252, doi:10.1029/JZ064i012p02239.
- Doxas, I., W. Horton, W. Lin, S. Seibert, and M. Mithaiwala (2004), A dynamical model for the coupled inner magnetosphere and tail, *IEEE Trans. Plasma Sci.*, *32*(4), 1443–1448, doi:10.1109/TPS.2004.833388.
- Feldstein, Y. I., and L. A. Dremukhina (2000), On the two-phase decay of the Dst variation, *J. Geophys. Res.*, *105*(17), 2813–2816.
- Horton, W., M. Mithaiwala, E. Spencer, and I. Doxas (2005), WINDMI: A family of physics network models for storms and substorms, in *Multi-Scale Coupling of Sun-Earth Processes*, edited by A. Lui, Y. Kamide, and G. Consolini, pp. 431–446, Elsevier, doi:10.1016/B978-0-444-51881-1/50032-0.
- Jordanova, V. K., L. M. Kistler, M. F. Thomsen, and C. G. Mouikis (2003), Effects of plasma sheet variability on the fast initial ring current decay, *Geophys. Res. Lett.*, *30*(6), 1311, doi:10.1029/2002GL016576.
- Kalegaev, V., and E. Makarenkov (2008), Relative importance of ring and tail currents to Dst under extremely disturbed conditions, *J. Atmos. Sol. Terr. Phys.*, *70*, 519–525, doi:10.1016/j.jastp.2007.08.029.

- Kamide, Y., and A. Chian (Eds.) (2007), *Handbook of the Solar-Terrestrial Environment*, Springer, Berlin, doi:10.1007/978-3-540-46315-3.
- Keika, K., M. Nose, S. Ohtani, K. Takahashi, S. P. Christon, and R. W. McEntire (2005), Outflow of energetic ions from the magnetosphere and its contribution to the decay of the storm time ring current, *J. Geophys. Res.*, *110*, A09210, doi:10.1029/2004JA010970.
- Kozyra, J. U., and M. W. Liemohn (2003), Ring current energy input and decay, *Space Sci. Rev.*, *109*(1–4), 105–131, doi:10.1023/B:SPAC.0000007516.10433.ad.
- Kozyra, J. U., M.-C. Fok, E. R. Sanchez, D. S. Evans, D. C. Hamilton, and A. F. Nagy (1998), The role of precipitation losses in producing the rapid early recovery phase of the great magnetic storm of February 1986, *J. Geophys. Res.*, *103*(A4), 6801–6814, doi:10.1029/97JA03330.
- Kozyra, J. U., M. W. Liemohn, C. R. Clauer, A. J. Ridley, M. F. Thomsen, J. E. Borovsky, J. L. Roeder, V. K. Jordanova, and W. D. Gonzalez (2002), Multistep *Dst* development and ring current composition changes during the 4–6 June 1991 magnetic storm, *J. Geophys. Res.*, *107*(A8), 1224, doi:10.1029/2001JA000023.
- Kunori, T., M. Nose, S. Taguchi, K. Hosokawa, M. R. Collier, and T. E. Moore (2007), Storm phase dependence of ion outflow: Statistical signatures obtained by IMAGE/LENA, *Geophys. Res. Lett.*, *34*, L18106, doi:10.1029/2007GL029877.
- Lee, D.-Y., L. R. Lyons, and G. D. Reeves (2005), Comparison of geosynchronous energetic particle flux responses to solar wind dynamic pressure enhancements and substorms, *J. Geophys. Res.*, *110*, A09213, doi:10.1029/2005JA011091.
- Lee, D.-Y., S. Ohtani, P. C. Brandt, and L. R. Lyons (2007), Energetic neutral atom response to solar wind dynamic pressure enhancements, *J. Geophys. Res.*, *112*, A09210, doi:10.1029/2007JA012399.
- Liemohn, M. W., and J. U. Kozyra (2005), Testing the hypothesis that charge exchange can cause a two-phase decay, in *The Inner Magnetosphere: Physics and Modeling*, *Geophys. Monogr. Ser.*, vol. 155, edited by T. Pulkkinen, N. A. Tsyganenko, and R. H. W. Friedel, p. 211, AGU, Washington, D. C.
- Liemohn, M. W., J. U. Kozyra, C. R. Clauer, and A. J. Ridley (2001), Computational analysis of the near-Earth magnetospheric current system during two-phase decay storms, *J. Geophys. Res.*, *106*, 29,531–29,542, doi:10.1029/2001JA000045.
- Maltsev, Y. (2004), Points of controversy in the study of magnetic storms, *Space Sci. Rev.*, *110*, 227–277, doi:10.1023/B:SPAC.0000023410.77752.30.
- Maltsev, Y. P., A. A. Arykov, E. G. Belova, B. B. Gvozdevskiy, and V. V. Safargaleev (1996), Magnetic flux redistribution in the storm time magnetosphere, *J. Geophys. Res.*, *101*(A4), 7697–7704, doi:10.1029/95JA03709.
- Mitchell, D. G., K. C. Hsieh, C. C. Curtis, D. Hamilton, H. D. Voss, E. C. Roelof, and P. C. son-Brandt (2001), Imaging two geomagnetic storms in energetic neutral atoms, *Geophys. Res. Lett.*, *28*(6), 1151–1154, doi:10.1029/2000GL012395.
- O'Brien, T. P., and R. L. McPherron (2000), An empirical phase space analysis of ring current dynamics: Solar wind control of injection and decay, *J. Geophys. Res.*, *105*(A4), 7707–7719, doi:10.1029/1998JA000437.
- O'Brien, T. P., R. L. McPherron, and M. W. Liemohn (2002), Continued convection and the initial recovery of *Dst*, *Geophys. Res. Lett.*, *29*(23), 2143, doi:10.1029/2002GL015556.
- Reiff, P. H., and J. G. Luhmann (1986), Solar wind control of the polar-cap voltage, in *Solar Wind-Magnetosphere Coupling*, edited by Y. Kamide and J. A. Slavin, pp. 453–476, Terra Sci., Tokyo.
- Skopke, N. (1966), A general relation between the energy of trapped particles and the disturbance field near the Earth, *J. Geophys. Res.*, *71*(13), 3125–3130, doi:10.1029/JZ071i013p03125.
- Siscoe, G. L., R. L. McPherron, and V. K. Jordanova (2005), Diminished contribution of ram pressure to *dst* during magnetic storms, *J. Geophys. Res.*, *110*, A12227, doi:10.1029/2005JA011120.
- Spencer, E., W. Horton, L. Mays, I. Doxas, and J. Kozyra (2007), Analysis of the 3–7 October 2000 and 15–24 April 2002 geomagnetic storms with an optimized nonlinear dynamical model, *J. Geophys. Res.*, *112*, A04S90, doi:10.1029/2006JA012019.
- Spencer, E., A. Rao, W. Horton, and M. L. Mays (2009), Evaluation of solar wind-magnetosphere coupling functions during geomagnetic storms with the WINDMI model, *J. Geophys. Res.*, *114*, A02206, doi:10.1029/2008JA013530.
- Takahashi, S., T. Iyemori, and M. Takeda (1990), A simulation of the storm time ring current, *Planet. Space Sci.*, *38*(9), 1133–1141, doi:10.1016/0032-0633(90)90021-H.
- Tsyganenko, N. A., and M. I. Sitnov (2005), Modeling the dynamics of the inner magnetosphere during strong geomagnetic storms, *J. Geophys. Res.*, *110*, A03208, doi:10.1029/2004JA010798.
- Wolf, R., R. Spiro, S. Sazykin, and F. Toffoletto (2007), How the Earth's inner magnetosphere works: An evolving picture, *J. Atmos. Sol. Terr. Phys.*, *69*, 288–302, doi:10.1016/j.jastp.2006.07.026.

W. Horton, Space and Geophysics Laboratory, University of Texas at Austin, RLM 11.320, 1 University Station C1500, Austin, TX 78712-1081, USA.

S. Patra and E. Spencer, Center for Space Engineering, Utah State University, Logan, UT 84321, USA. (sunswadesh@yahoo.co.in)

J. Sojka, CASS, Utah State University, 4405 Old Main Hill, SER Bldg., Rm. 246, Logan, UT 84322-4405, USA.